JOURNAL OF GEOPHYSICAL RESEARCH, VOL. 105, NO. C8, PAGES 19,535–19,550, AUGUST 15, 2000

Seasonal to interannual variability from expendable bathythermograph and TOPEX/Poseidon altimeter data in the South Pacific subtropical gyre

Mary Cait McCarthy, Lynne D. Talley, and Dean Roemmich

Scripps Institution of Oceanography, University of California San Diego, La Jolla

Abstract. Estimates of dynamic height anomalies from expendable bathythermograph (XBT) and TOPEX/Poseidon (T/P) sea surface height (SSH) measurements were compared along a transect at ~30°S in the South Pacific. T/P SSH anomalies were calculated relative to a 5 year time mean. XBT dynamic height was calculated relative to 750 m using measured temperature and an objectively mapped climatological temperature-salinity relationship. The anomaly was obtained by subtracting out an objectively-mapped climatological dynamic height relative to 750 m. XBT temperature sections show evidence of a double-gyre structure, related to changes in shallow isopycnals near the gyre's center. XBT dynamic height and T/P SSH anomalies compare well with an RMS difference of 3.8 cm and a coherence above 0.7 for scales larger than 300 km. The differences between the two measures of dynamic height yield systematic patterns. Time-varying spatial averages of the differences are found to be related to changes in Sverdrup transport, zonal surface slope differences, and the 6°C isotherm depth. Higher zonally averaged altimetry SSH than zonally averaged XBT height and larger northward transport from altimetry SSH than from XBT height correspond to gyre spinup determined from Sverdrup transport changes. This implies mass storage during gyre spinup due to the phase lag between the Ekman pumping and the full baroclinic Sverdrup response. Increases in the spatially averaged differences and zonal slope differences, associated with gyre spinup, correspond to shoaling in the 6°C isotherm depth, requiring deep baroclinic changes out of phase with the 6°C isotherm depth changes.

1. Introduction

Sea surface height (SSH) changes come from both dynamical and nondynamical responses to various forcing mechanisms including buoyancy, tidal, and wind forcing as well as atmospheric pressure. Contributions to SSH can be divided into four categories relating to different forcing mechanisms: a response to atmospheric pressure, a barotropic or bottom pressure portion related to changes in column-integrated mass, a baroclinic portion that includes steric changes in the upper water column, and differential mass changes throughout the rest of the water column that create geostrophic shear. Several studies have sought to understand the relative importance of the contributions to SSH changes [*Pattullo et al.,* 1955; *Gill and Niiler,* 1973; *Stammer,* 1997b; *Wunsch and Stammer,* 1997]. After removing the nondynamical atmospheric or inverted barometric contribution to sea level [*Gill and Niiler,* 1973; *Fu and Pihos,* 1994] the largest contribution to seasonal SSH change is the steric heating and cooling of the upper layer [*Gill and Niiler,* 1973; *Stammer and Wunsch,* 1994; *Minster et al.,* 1995; *Stammer,* 1997b]. Because the steric response is coherent over such large scales, it has only a small dynamical effect. Ocean dynamics, however, are influenced by the seasonal baroclinic and barotropic contributions to sea level change. *Gill and Niiler* [1973] suggest that the baroclinic and barotropic responses to Ekman pumping changes are approximately equal at 30° latitude with the baroclinic portion dominating equatorward of 30° and the barotropic portion dominating poleward.

Except for localized direct measurements of SSH (also called sea level) by tide gauges, SSH has been approximated by calculations of dynamic height from temperature, salinity, and pressure measurements. Dynamic height is relative to an unknown but estimated geopotential surface and thus measures all of the baroclinic contributions above the reference surface to SSH while approximating any barotropic effects like tides, atmospheric pressure, and barotropic flows. SSH measures dynamic height plus the barotropic effects. Sorting out various contributions to SSH and their relation to dynamic height is a complex task, which has

Paper number 2000JC900056.
0148-0227/00/2000JC900056$09.00

been aided by the satellite altimeter's regular large-scale measurements of absolute SSH anomalies. In order to make progress in understanding these contributions to SSH this work examines the similarities and differences between SSH anomaly estimates from the TOPEX/Poseidon (T/P) altimeter and dynamic height anomaly estimates relative to 750 m from a high-resolution expendable bathythermograph (XBT) line in the South Pacific (~30°S). This transect traverses the poleward side of the anticyclonic subtropical gyre [*Reid,* 1986, 1997] and is bisected by the Subtropical Front, which crosses 30°S between 110° and 90°W [*Stramma et al.,* 1995]. The mean cruise track lies in the region of minimum wind stress and maximum wind stress curl [*Trenberth et al.,* 1990] and S. Wijffels et al. (On the circulation of the subtropical South Pacific Ocean, submitted to *Journal of Geophysical Research,* 2000, hereinafter referred to as Wijffels et al. submitted manuscript, 2000).

In the subtropical South Pacific gyre, *Reid* [1986] suggests that the barotropic component of flow is small, while *Fu and Davidson* [1995] find a relatively large barotropic response to wind forcing in the southeast, south of 30°S. Thus the dynamical barotropic contribution to sea level is expected to be small except possibly in the eastern portion of the basin. Several studies also suggest that a double maximum in SSH exists in the South Pacific, similar to that observed in the North Pacific [*Hautala et al.,* 1994]. Wijffels et al. (submitted manuscript, 2000) observe the double maximum due to shallow isopycnal slope reversal near 110°W along the World Ocean Circulation Experiment (WOCE) hydrographic section at 32°S. *Huang and Qiu* [1998] also capture this feature using a model forced with climatological wind stress and winter mixed layer density and depth. In SSH this feature is seen as a slight second SSH maximum in the eastern third of the basin. Permanent mesoscale features appear in the mean dynamic height, including both the East Auckland Current and the warm-core East Cape Eddy [*Roemmich and Sutton,* 1998]. North of 29°S, annual SSH variability is influenced by the local isopycnal response to Ekman pumping and by the gyre's intensity and center location variations as shown by *Roemmich and Cornuelle* [1990] and *Morris et al.* [1996] in the western South Pacific. Dominance of annual variations in the thermocline does not extend south of 29°S [*Roemmich and Cornuelle,* 1990], suggesting a period other than annual for most of the thermocline variability along our transects.

Since the 1992 launch of the T/P altimetric satellite, several studies [*Mitchum,* 1994; *Nerem et al.,* 1994; *White et al.,* 1994; *Gilson et al.,* 1998] have clarified the nature of the T/P SSH data and its relationship to more traditional measures of SSH and dynamic height. *Gilson et al.* [1998] find good agreement between XBT dynamic height anomalies and T/P SSH anomalies in the North Pacific. The two types of data have an RMS difference of 5.2 cm, a coherence of 0.89 for scales > 500 km, and a robust statistical relationship that can be used to construct temperature sections to 800 m from regressions of T/P data. T/P, in fact, has achieved remarkable accuracy in its SSH anomaly measurements, making it a viable tool for variability studies.

Comparing T/P SSH wavelength spectra to classical spectra yields further insight into the statistics of the T/P data. In a global analysis of T/P SSH data, *Stammer* [1997a], like previous authors [*Le Traon et al.,* 1994; *Wunsch and Stammer,* 1995], showed flat spectra at long wavelengths and spectra proportional to k^{-5} for shorter wavelengths, with the cutoff wavelength between the Rhines scale ($\sqrt{U/\beta}$) and the first baroclinic radius of deformation. Such results agree well with theory since the k^{-5} falloff is the dependence expected for SSH spectra of geostrophic turbulence [*Charney,* 1971]. This falloff rate should change for scales greater than the Rhines scale, where the small- to large-scale cascade of turbulent energy is arrested by Rossby wave propagation [*Rhines,* 1975]. *Stammer* [1997a] used T/P data to show that the global average falloff was closer to k^{-4}, with the falloff in the center of the subtropical gyre tending toward k^{-3}. These results suggest that the k^{-5} scale serves as a general guideline and that in practice, the expected sprectra will have a a steeper falloff rate at scales smaller than the Rhines scale.

Less frequently employed are the differences between the various measures of SSH as a tool for gaining added insight into the dynamics that govern the system. Since XBTs only measure contributions between the surface and 750 m while the T/P measurement observes effects of the entire water column on SSH we expect differences between their estimates even if both instruments were perfect. This study seeks first to establish the similarity between the measures of XBT dynamic height and T/P SSH and second to understand the systematic differences between them.

2. Methods

XBT sections were sampled approximately quarterly from August 1993 to January 1998 along the WOCE high-resolution line PX50 from Valparaiso, Chile, to Auckland, New Zealand. A total of 17 transects were made in collaboration with the Chilean navy. The data were taken aboard the *Joana Bonita* until the end of 1995 and then aboard the *Asian Challenger.* Each ship accommodated a scientist who used an automatic XBT launcher to sample approximately every 2 hours, resulting in a horizontal resolution of ~50 km, with spacing as fine as every 10-15 km near the coasts. Sippican Deep Blue XBTs were used along PX50 and sampled to over 800 m depth, providing a record of subsurface variability along the transect. Each 17 day transect usually yielded more than 250 profiles. Most cruises also included sparse sampling with expendable CTDs (XCTDs), totaling over 180 profiles with both temperature and salinity during the 5 year period.

Table 1. Double-Gyre Structure

Cruise	Cruise Dates	Number of Observations	Double Gyre?[a]	Isopycnal Depth Minimum
9308	Aug. 5-22, 1993	240	yes	120° - 115°W
9401	Jan. 24 to Feb. 9, 1994	295	yes	130° - 125°W
9404	April 19 to May 6, 1994	159	yes	130° - 125°W
9407	July 31 to Aug. 16, 1994	305	no	...
9410	Oct. 29 to Nov. 14, 1994	270	no	...
9501	Jan. 28 to Feb. 12, 1995	312	no	...
9504	April 25 to May 5, 1995	261	...	...
9507	July 25 to Aug. 10, 1995	266	yes	125° - 120°W
9510	Oct. 28 to Nov. 13, 1995	163	yes	115° - 110°W
9604	April 7-19, 1996	260	...	...
9607	July 21 to Aug. 5, 1996	271	...	...
9611	Nov. 9-22, 1996	265	yes	120° - 115°W
9702	Feb. 7-19, 1997	266	no	...
9705	May 8-22, 1997	275	...	...
9708	Aug. 3-18, 1997	271	...	...
9710	Oct. 22 to Nov. 5, 1997	266	no	...
9801	Jan. 9-24, 1998	268	...	...

[a]Only for cruises that are approximately zonal.

Plate 1 shows the tracks of the 17 cruises considered. Only four of the cruises were exactly repeating, complicating the analysis since the variability is a function of both time and space. Cruises are named by four numbers consisting of the two-digit year and the two-digit month in which they occurred (e.g., the August 1993 cruise is called 9308). Table 1 provides descriptive information for each cruise, including cruise durations and the number of observations. For comparison with the T/P SSH anomaly we estimate the dynamic height anomaly from the XBT temperature data by combining it with a climatological temperature-salinity (T-S) relationship and then subtracting a climatological dynamic height. Because of the variable nature of the cruise track, the T-S and the dynamic height climatologies were created for the region between Chile and New Zealand, from 20° to 40°S.

For the T-S climatology all available historical bottle data for the region were collected from the Scripps Institution of Oceanography (SIO) Hydrosearch data archives and were combined with WOCE CTD data and PX50 XCTD data. The data were objectively analyzed in temperature, longitude, and latitude space (Figure 1). Figure 2 shows the salinity section and dynamic height relative to 750 m at 32°S from the WOCE P6 cruise in 1992 Wijffels et al. (submitted manuscript, 2000). The main salinity features that a climatology must capture include the salty surface layer in the western and central portion of the section, the strong front between 90° and 80°W, the fresh tongue to the east of the front, and the low-salinity Antarctic Intermediate Water in the eastern basin below 500 m. A grid spacing of 5° longitude by 2° latitude was found to capture these features to the extent possible with the available data coverage. Mapped data were then linearly interpolated to XBT locations. By comparing two estimates of dynamic height from PX50 XCTD data using salinity obtained from the mapped T-S and the measured salinity we found the RMS difference to be 1.8 cm, with the largest errors in the mixed layer. While this error estimate may be low since the XCTD data were part of the mapping, it confirms that the errors due to salinity likely do not exceed the T/P error (which is ~4.3 cm and is discussed below).

Other XBT dynamic height errors result from the depth estimation and the temperature sensor. To re-

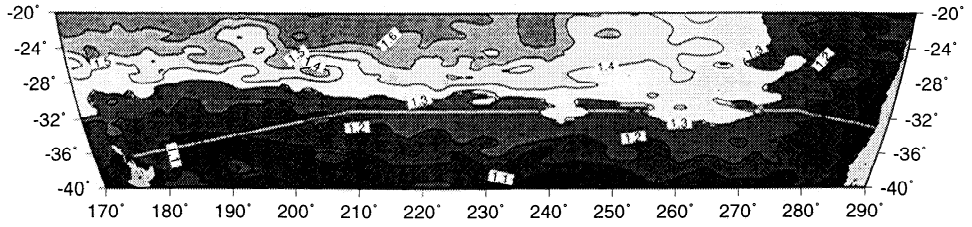

Figure 1. Objective map of mean SSH relative to 750 m from all available historic data. The white line marks the average XBT cruise track.

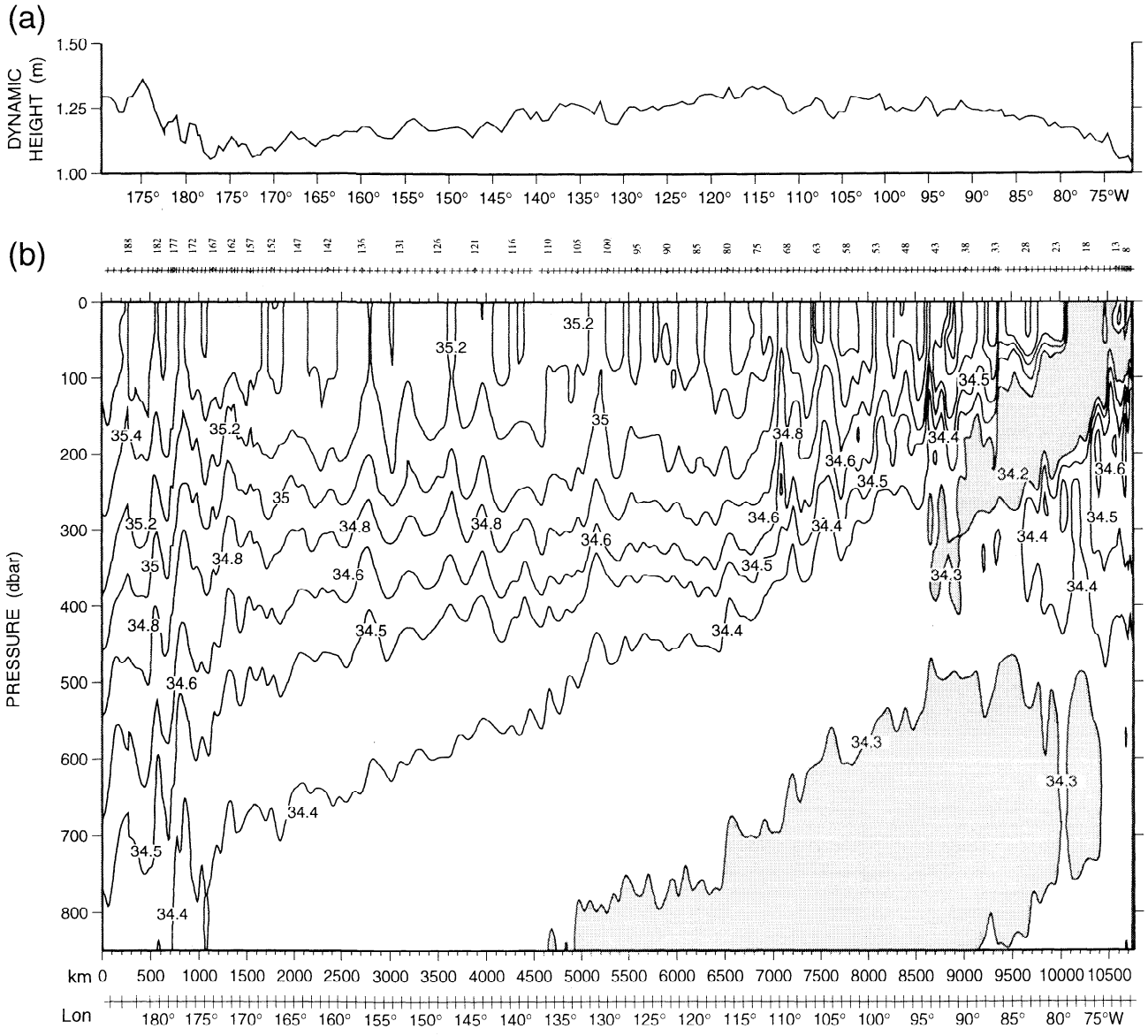

Figure 2. (a) Dynamic height relative to 750 m and (b) salinity section at 32°S from the WOCE P6 cruise (Wijffels et al., submitted manuscript, 2000). Salinities < 34.3 are shaded.

duce the depth error to 1% of the depth, the linear fall rate correction suggested by *Hanawa et al.* [1995] was applied to all XBT depth data. Thermistors were calibrated with a residual error of ~0.05°C [*Roemmich and Cornuelle,* 1987]. If both temperature and depth errors are coherent throughout the water column, the resulting RMS dynamic height error is 1.25 cm [*Gilson et al.*, 1998]. Since both errors are random, the error can be reduced by averaging.

Climatological dynamic height relative to 750 m was calculated from all the data used in the T-S relation in combination with all historical XBT casts > 750 m gathered from the National Oceanographic Data Center (NODC) and Global Temperature-Salinity Pilot Project (GTSPP) databases and with the PX50 XBT data. The climatological T-S relation was used to obtain the salinity necessary for the XBT dynamic height calculation. Before the climatological dynamic height was mapped the data were binned into 1° latitude by 2° longitude regions and quality controlled by removing any values falling more than 2 standard deviations away from the mean. The quality control process was then repeated to minimize the effect of far outliers. Approximately 95% of the data met the quality control standard, and these data were objectively mapped on a 0.5° longitude by 0.25° latitude grid. Dynamic height decorrelation length scales of 500 km zonally and 200 km meridionally capture the permanent mesoscale features (Figure 1). The mean may be slightly biased toward summer values (dynamic height too large) because of more summer sampling, as found by *Roemmich and Sutton* [1998] in a similar mapping. The error in the mapped esti-

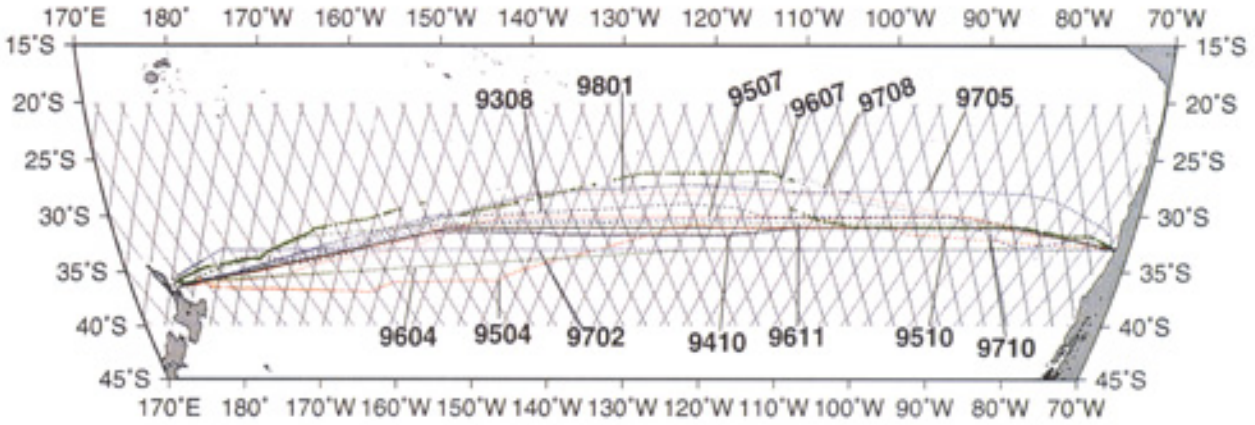

Plate 1. PX50 XBT cruise locations and TOPEX/Poseidon altimeter ground tracks. Cruise naming is described in text. Cruises 9401, 9404, 9407, and 9501 are exactly repeating and represented by the solid black line.

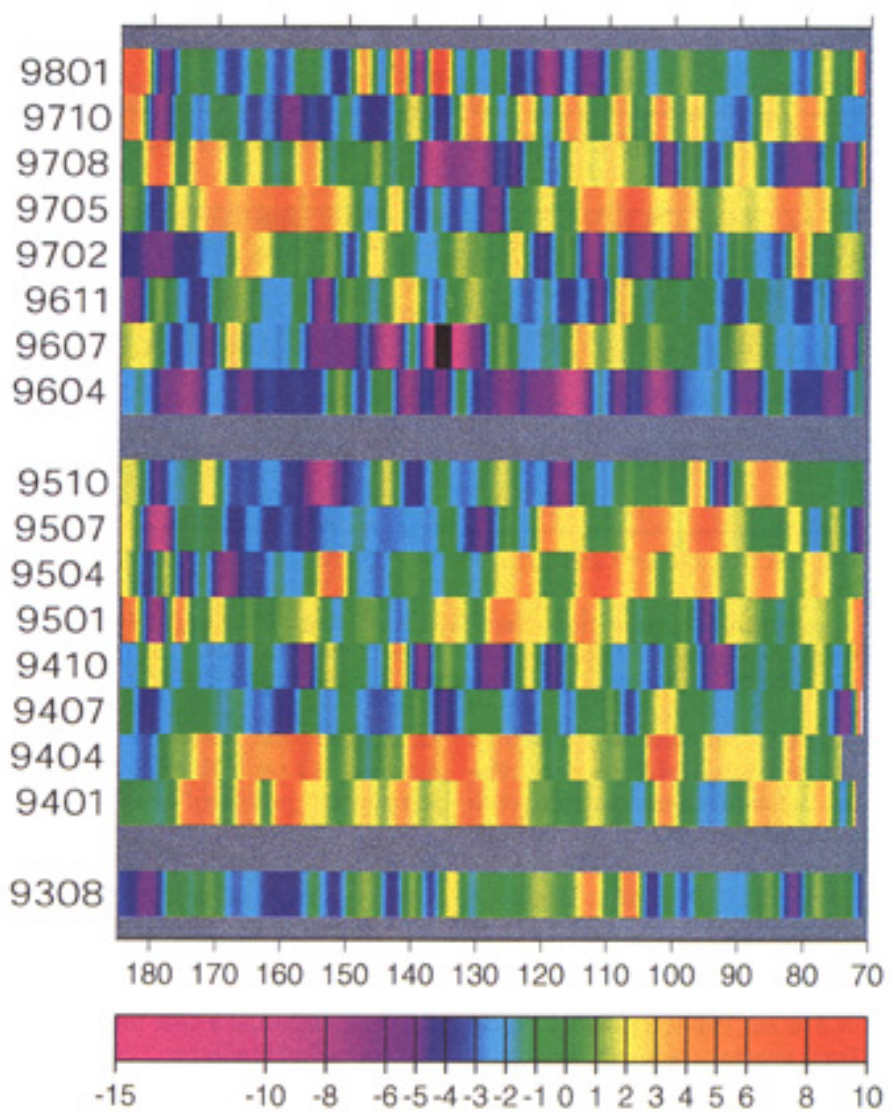

Plate 2. Time-longitude plot of XBT minus T/P SSH anomalies (in centimeters) with 5° smoothing. Note that the sign convention here is opposite that of Figures 7, 9, and 11.

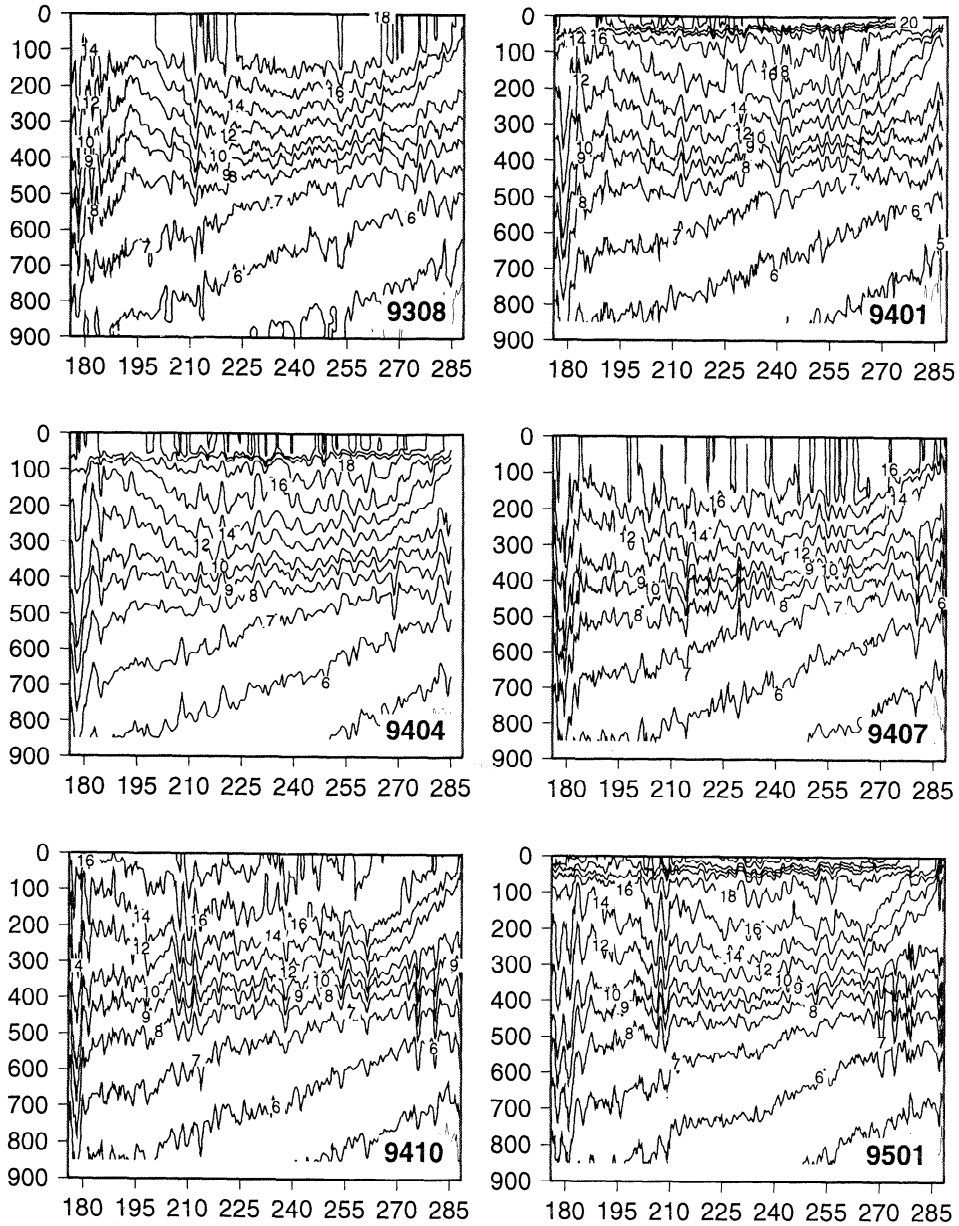

Figure 3. Temperature sections from the PX50 XBT line. Bold numbers in the lower right corners represent the cruise numbers. See Plate 1 for cruise locations.

mate of the mean is only 0.25 cm because of the good data coverage and the large assumed scales of decorrelation. The climatological mean was interpolated to each XBT station location and subtracted from the dynamic height calculated there from the measured temperature and the mapped climatological T-S relation. The total RMS error in a point measurement anomaly is 2.21 cm.

T/P data are collected on approximately meridional tracks with an along-track resolution of 6.2 km, an equatorial track spacing of 316 km (Plate 1), and a repeat cycle of 9.916 days. Track spacing decreases toward the poles. Our data set is from the Jet Propulsion Laboratory in Pasadena, California, where the data have been corrected for instrumental and atmospheric errors [*Fu et al.*, 1994] and the inverse barometer effect. In addition, the tidal signal [*Li et al.*, 1996] and geoid [*Tapley et al.*, 1996] have been removed. The resulting RMS error is ~4.3 cm [*Gilson et al.*, 1998]. At SIO the data were further processed by removing far outliers and applying a three-point running mean to along-track data. Residual temporal means are removed from each data location. We then objectively mapped the data to a 1/6° grid at 10 day intervals. Finally, the mapped data were linearly interpolated to XBT station locations and times. The T/P mapping introduces an RMS error of 3.07 cm, while the 5 year mean compared to the longer XBT mean adds another 2 cm RMS. The resulting point measure of the T/P anomaly has an RMS error of 5.65 cm.

Wavenumber spectra and coherence and phase between the XBT and T/P space series were calculated and time-averaged, yielding 34 degrees of freedom. Dif-

ferences between anomalies of XBT dynamic height and T/P SSH were analyzed after both data types were interpolated to 0.1° zonal resolution in order to weight equally coastal and open ocean differences. Differences were spatially averaged along the transect and compared to the zonally integrated Sverdrup transport anomaly at 32°S from the eastern boundary to 180°E and to the spatially averaged 6°C isotherm depth anomaly. The Sverdrup transport was calculated from the daily National Centers for Environmental Prediction (NCEP) reanalysis momentum flux data, transport $= \int (\frac{1}{\rho\beta})(\frac{\partial \tau^y}{\partial x} - \frac{\partial \tau^x}{\partial y})dx$, averaged over the 30 days before the last day of each XBT transect with a 7 year (1991-1997) mean removed. Transport implied by the slope difference between T/P and XBT was calculated by fitting two lines through the SSH data. The endpoints of each line were determined from minima and maxima in the original (not anomaly) XBT data for each cruise. The first line was fit between the first SSH minimum west of the East Cape Eddy off of New Zealand and the midgyre SSH maximum. The second line was fit from the midgyre maximum to the coast of Chile. The 6°C isotherm depth anomalies were obtained by subtracting a climatological 6°C isotherm depth (created in the same manner as the dynamic height climatology) from the measured XBT 6°C isotherm depth at each XBT station location. The depth anomalies were also interpolated to 0.1° longitudinal spacing and spatially averaged.

3. Results and Discussion

3.1. Temperature Sections, Dynamic Heights, and the Double Gyre

Figure 3 shows the XBT temperature sections. As mentioned, the analysis is complicated by the fact that

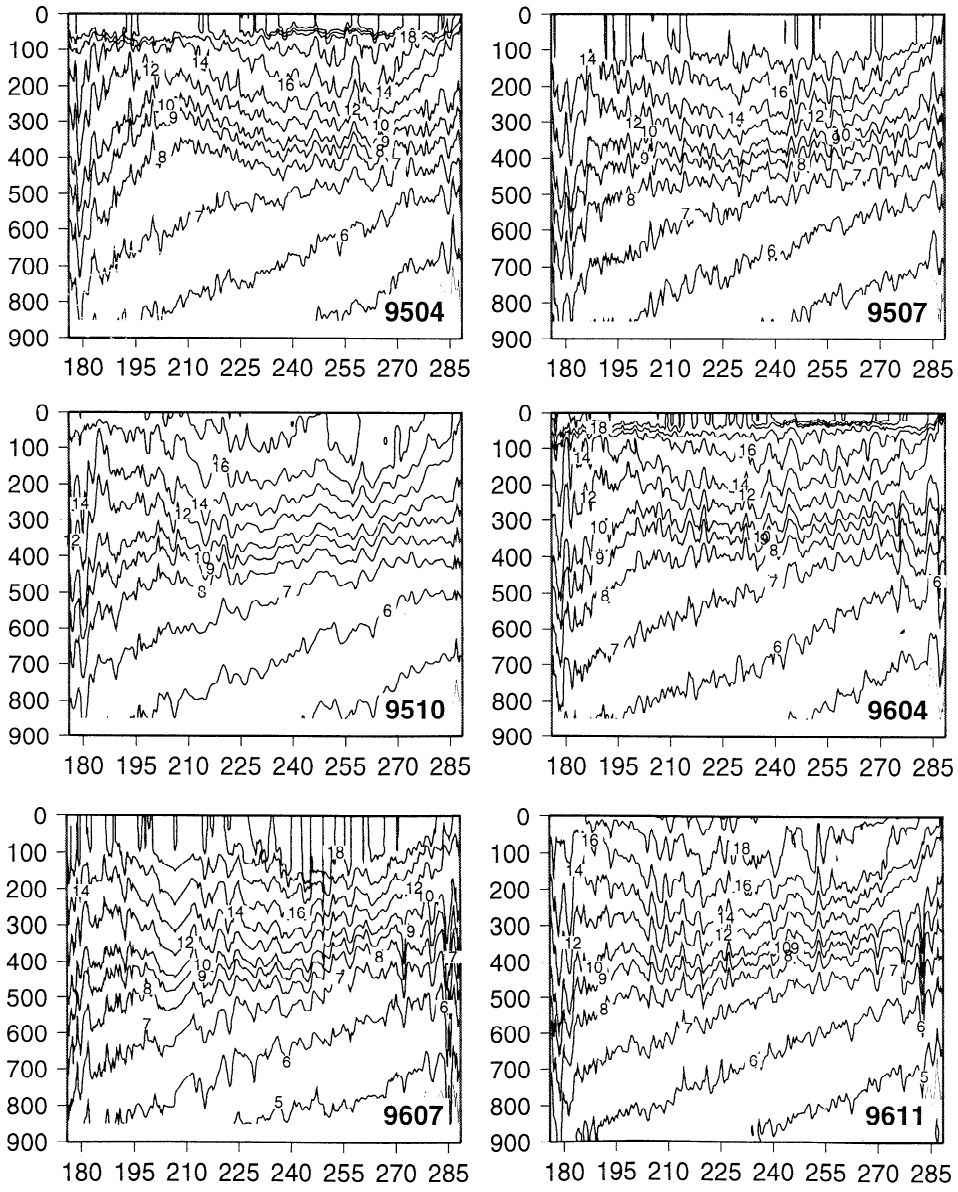

Figure 3. (continued)

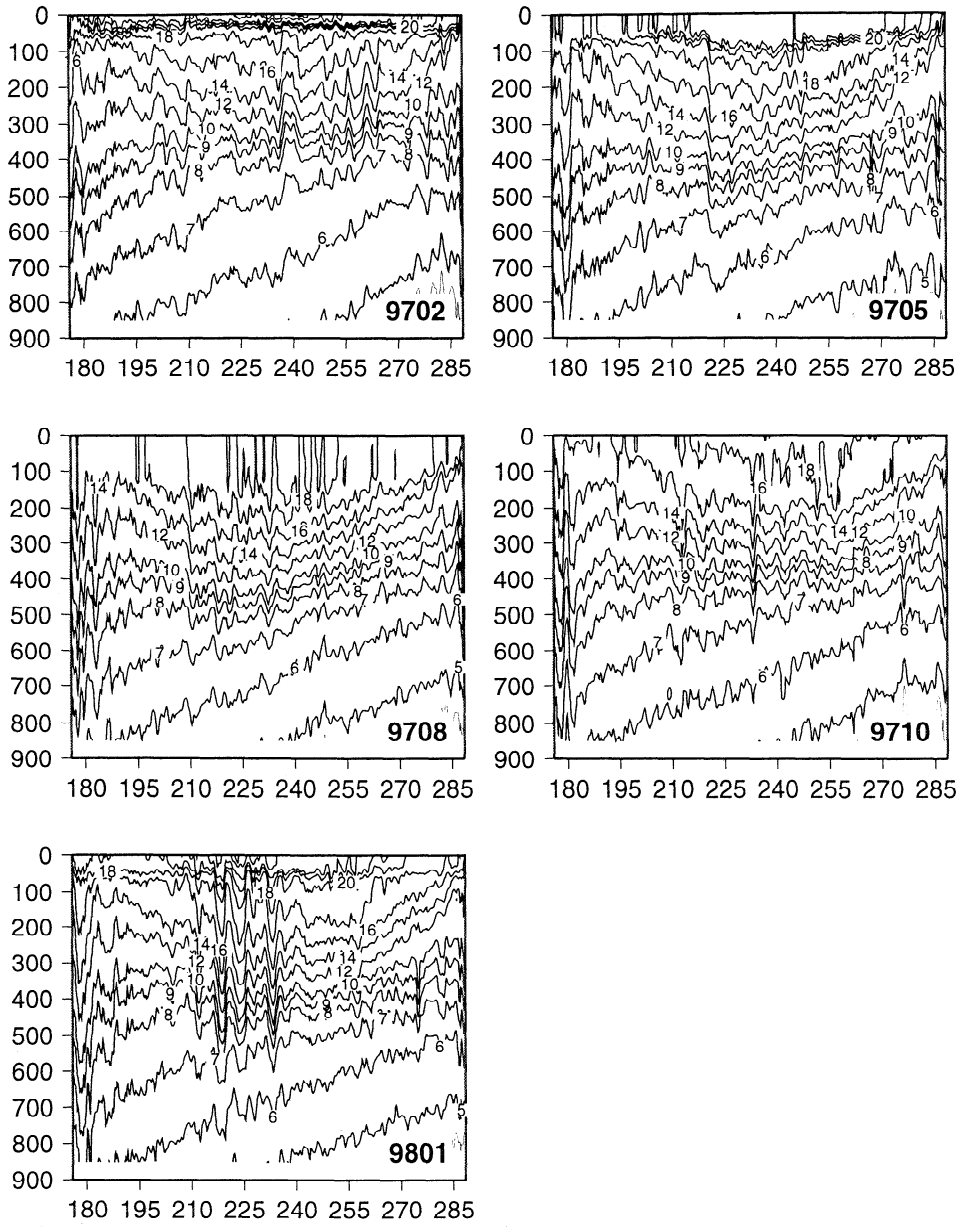

Figure 3. (continued)

the locations vary in time and space. However, a few observations can be made about the general variability of the gyre. The most obvious change from cruise to cruise occurs in the upper water column as the deep, cooler winter mixed layer changes to a warmer, stratified seasonal thermocline and vice versa. Even with the track location variation, the annual cycle is evident.

From the temperature sections and the resulting dynamic height relative to 750 m (Figure 4, thick solid line) some of the cruises show evidence of the double gyre by the shoaling and deepening of the isotherms in the upper 400 m near the center of the section. A similar structure was previously observed by *Huang and Qiu* [1998] and Wijffels et al. (submitted manuscript, 2000) for the WOCE section at 32°S (Figure 2a). Confirming these observations, the dynamic height and shallow isotherm depth minima occur between 130° and 110°W. PX50 observations suggest that while the double-gyre feature may exist in the mean as previously observed, it is not a permanent feature. The first six cruises are approximately along the same track, and although the first three cruises exhibit evidence of the double structure, the last three do not. *Huang and Qiu*'s [1998] analytical model indicates that in the mean any approximately zonal section between 25° and 35°S should show the feature. Considering only approximately zonal cruises to avoid possible meridional variations, Table 1 tallies which cruises have the double-gyre structure and, when present, the location of the minimum dynamic height in the PX50 data. The double gyre was judged present when there was a break of more than 5° in the monotonic upward slope of isopycnals in the eastern half of

the gyre. The location at which the slope changes from upward to downward is noted as the dynamic height minimum. The lack of a double gyre structure in every cruise may be due to eddy variability overwriting the signal, but the persistence of periods with and without the structure indicates that the feature's existence along this transect is periodic or occasional rather than permanent. In the mean a hint of its existence can been seen throughout the latitudinal extent of gyre (Figure 1).

In the North Pacific, *Hautala et al.* [1994] found a double-gyre structure associated with the salinity front formed by the shallow salinity minimum abutting saltier waters to the west of and above it. The eastern South Pacific also has a shallow salinity minimum front near the location of the dynamic height minimum, similar to that originally mapped by *Sverdrup et al.* [1942] (Figure 2). If this is related to the double gyre's existence, it might provide an explanation for the occasional lack of the double gyre in the XBT temperature data since the zonal movement of the low-salinity tongue is impossible to represent with the climatological T-S relation. In this case the T/P SSH data should show the double gyre since they do not have the same salinity errors as the XBT dynamic height data do. The shaded line on Figure 4 is the T/P anomaly added to the climatological dynamic height relative to 750 m (the thin solid line). The T/P SSH shows times when the double gyre is present and times when it is absent, confirming XBT results. The feature's intermittency appears to be real and not due the fresh tongue's movement. The zonal distribution of XBT dynamic height and T/P SSH RMS variability (Figure 5) shows that both have increased variability between 160° and 120°W, the location of the western dynamic height maximum. This suggests that the double-gyre feature originates in the central portion of the gyre from isopycnal movement in the upper ocean, rather than at the eastern boundary because of salinity changes.

3.2. Statistical Comparison Between XBT and T/P Observations

From Figure 4 we have already seen the good visual agreement between the XBT dynamic height and T/P SSH. Their RMS difference across the section is 3.8 cm,

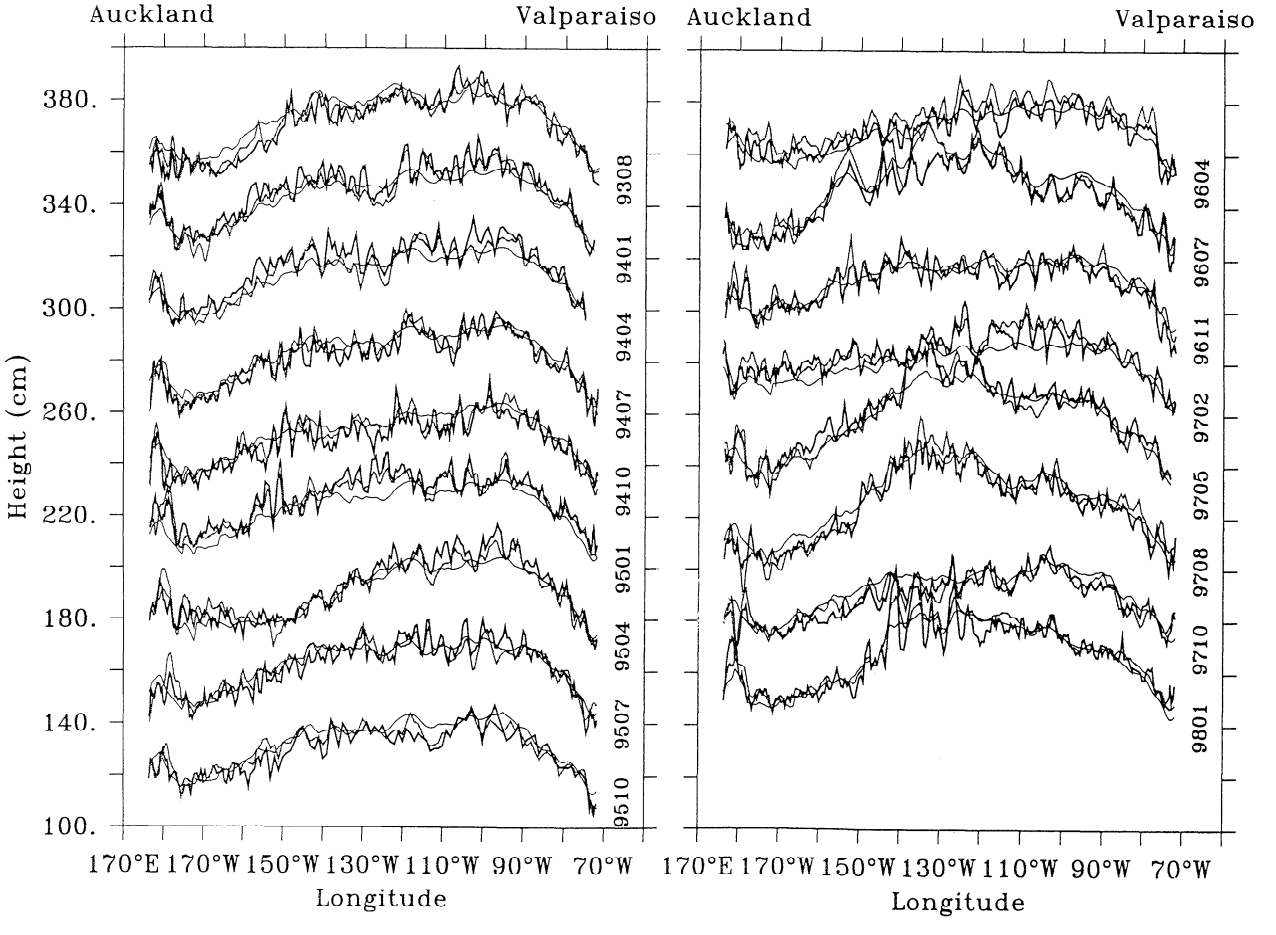

Figure 4. Climatological dynamic height relative to 750 m (thin solid line), PX50 XBT dynamic height relative to 750 m (thick solid line), and T/P SSH plus climatological dynamic height relative to 750 m (shaded line) at each PX50 cruise track and time. See Plate 1 for cruise locations.

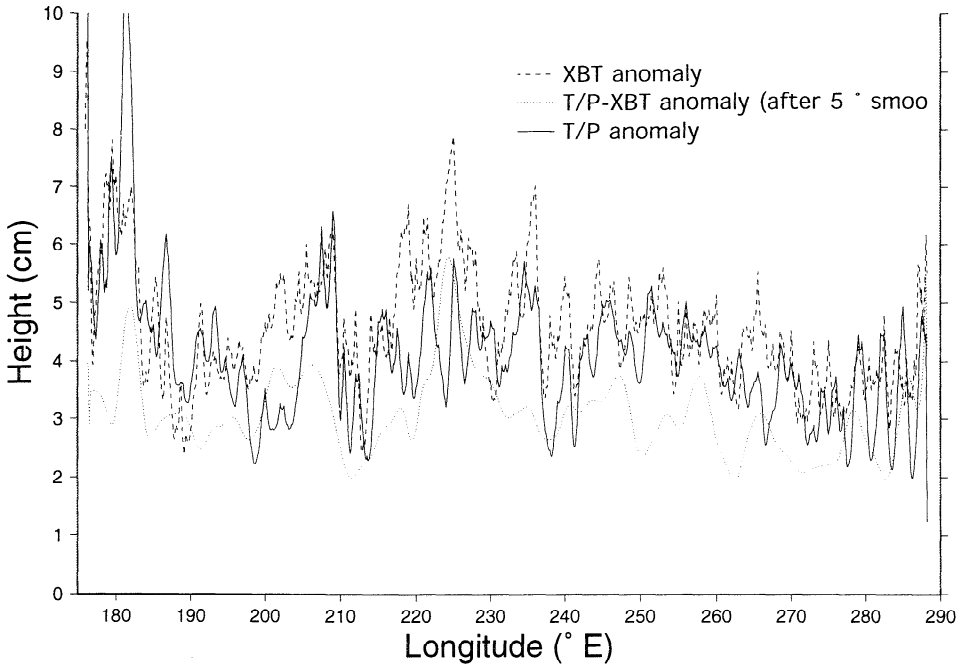

Figure 5. RMS variability versus longitude of XBT dynamic height anomaly (dashed line), T/P SSH anomaly (solid line), and the difference between T/P SSH and XBT dynamic height anomaly after 5° smoothing (dotted line).

with differences distributed generally evenly in longitude (Figure 5). Note that RMS differences were calculated from the original interpolated data and not from the smoothed data. Differences are slightly higher at the coasts and between 140° and 130°W, where the RMS dynamic heights of each of the individual measures is also high. This lack of large local differences between the measures confirms that the T-S relationship used for XBT salinity is consistently accurate across the basin. It also suggests that no particular portion of the basin is more dominated by barotropic motions as these motions would give rise to large local differences. The 3.8 cm RMS difference is 1.4 cm smaller than that found by *Gilson et al.* [1998] for the North Pacific because of the South Pacific's lower overall variability [*Stammer,* 1997a].

The zonal wavenumber spectra, coherence, and phase of the XBT dynamic height and T/P SSH anomalies are shown in Figure 6. The spectra compare well both with each other and with classical spectra [*Charney,* 1971; *Rhines,* 1979]. They are nearly flat at long wavelengths, and the slope steepens for wavelengths shorter than ~200 km (Rhines scale~100 km at 30°S [*Stammer,* 1997a]). At shorter scales the falloff is k^{-3}, less steep than the canonical k^{-5} but similar to the midgyre falloff rate found by *Stammer* [1997a]. The dashed line on Figure 6 is the k^{-3} slope. T/P energy falls off more quickly than that of the XBT since its actual sampling scale is ~200 km zonally. Artificial smaller-scale energy is due to the interpolation discussed previously. The coherence between the T/P and XBT is ~0.7 (significant within the 95% confidence limits) for scales > 300 km, and the phase of these scales is near zero. The coherence is lower than that of the North Pacific [*Gilson et al.,* 1998] either because the non-exactly repeating tracks produce a degraded average or because of the region's lower energy. Nevertheless, the two measures compare well, with the RMS difference between them being smaller than the estimated error for the T/P instrument alone. Combining the individual error estimates of T/P and XBT anomalies gives an RMS error of 4.27 cm for each point measure of their difference. Using the 34 degrees of freedom for the 17 cruises reduces the error to 1.04 cm. Even if our error estimate is low, it is still well below the observed RMS variability of 3.8 cm, indicating that part of the difference is indeed due to dynamics.

3.3. T/P and XBT Dynamic Height Anomaly Differences

A time-longitude plot of the differences between T/P and XBT anomalies (Plate 2) shows that the differences are not localized spatially. This confirms the assertion that neither errors in the mean nor errors in the salinity are dominating the pattern. Plate 2 also illustrates that the most pronounced pattern is the set of zonally coherent anomalies changing with time.

Our first analysis is a comparison of the transport implied by the T/P minus XBT differences with the wind-driven Sverdrup transport to determine if the ocean response is more barotropic than can be observed by the XBTs. Although the differences are noisy (Plate 2), a positive correlation is found between the zonal slope differences and the Sverdrup transport (Figure 7), in-

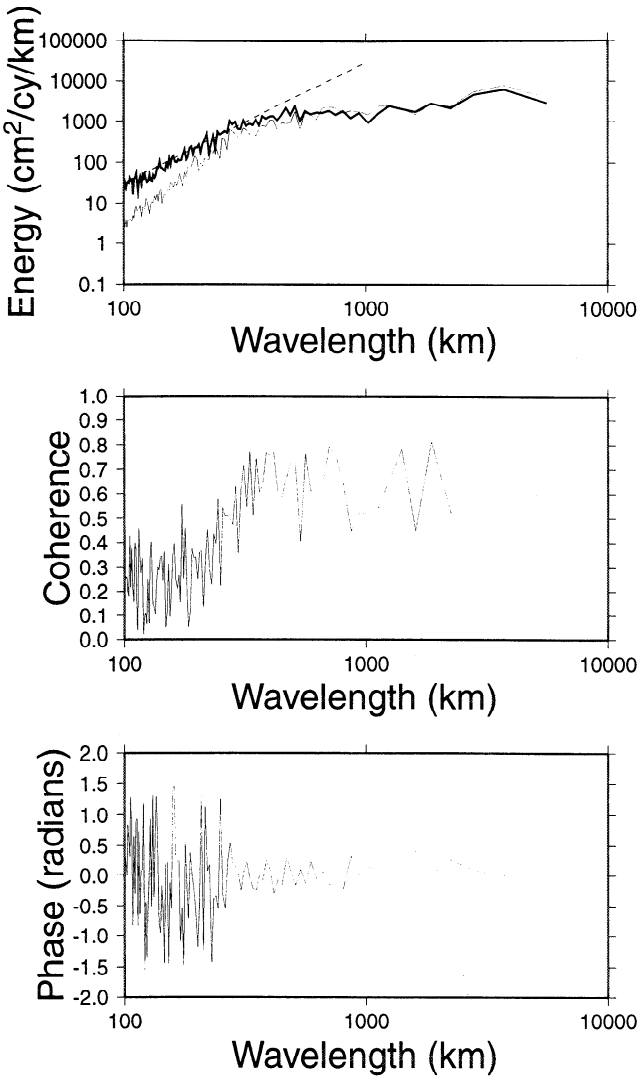

Figure 6. (a) Zonal wavenumber spectra of XBT dynamic height anomaly (thick line) and T/P SSH anomaly (thin line); the k^{-3} slope is plotted as a dashed line. (b) Coherence between space series of XBT dynamic height and T/P SSH anomalies versus wavelength. (c) Phase between space series of XBT dynamic height and T/P SSH anomalies versus wavelength.

dicating that indeed, the ocean response is deeper and stronger than is revealed by the XBTs alone. There is a suggestion of a lagged ocean response at a timescale less than the nominal 3-month sampling interval, although the sparse temporal sampling does not permit a lag to be identified very precisely. Because the slope calculation was somewhat dependent on choice of endpoints and because of the zonally coherent anomalies of Figure 7, we next examined basin averages.

The T/P and the XBT spatially averaged dynamic height anomalies (Figure 8) track each other well in sign, with both showing a strong seasonal cycle because of steric heating and cooling of the upper water column. Previous investigations have also found T/P SSH to capture adequately the seasonal cycle [*Stammer and Wunsch,* 1994; *Stammer,* 1997b], with average seasonal variability in the Northern Hemisphere 2 times larger than that of the Southern Hemisphere. *Gilson et al.* [1998] confirmed that XBT and T/P seasonal cycles compare well in the North Pacific, and we find the observed ranges of the XBT dynamic height and T/P SSH seasonal cycles are very comparable. This suggests that the hemispheric difference is not due to larger errors in either hemisphere. *Stammer* [1997b] also found that the steric response measured by T/P in the South Pacific agreed in magnitude with surface heat flux data but lagged in phase. Such an effect could not be detected by our data and could be due to poor atmospheric measurements in the Southern Hemisphere.

In taking the difference between XBT dynamic height and T/P SSH anomalies (Figure 9a), both the steric heating/cooling, which is confined to the upper 200 m [*Gill and Niiler,* 1973], and the baroclinic contribution above 750 m are removed since both measures observe these components. Therefore the differences can arise from either deep baroclinic contributions, barotropic contributions, and/or instrument noise. If the differences between the two measures of dynamic height were due only to random instrument noise, their spatial average would be expected to be very nearly zero. However, spatially averaged differences are of the order of 2 cm and are as large as 4 cm, which is of the order of the difference between the observed RMS variability and the

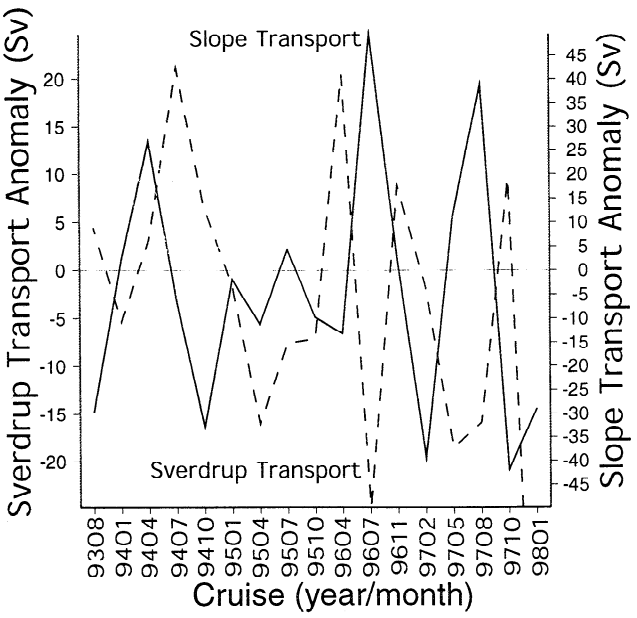

Figure 7. Time-dependent meridional transport implied by the slope of T/P minus XBT SSH anomalies (solid line) and Sverdrup transport anomaly at 32°S (dashed line) determined from the winds in the South Pacific subtropical gyre. Positive anomalies indicate more northward transport, and negative anomalies indicate less northward transport. The slope transport is scaled by an arbitrary choice of distribution of the additional transport over a layer 1000 m thick.

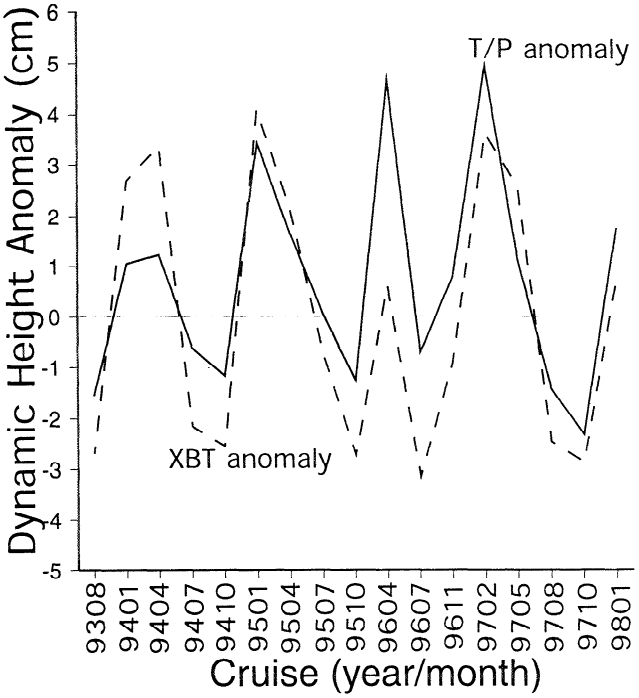

Figure 8. Time-dependent spatial averages of T/P SSH (solid line) and XBT dynamic height (dashed line) anomalies.

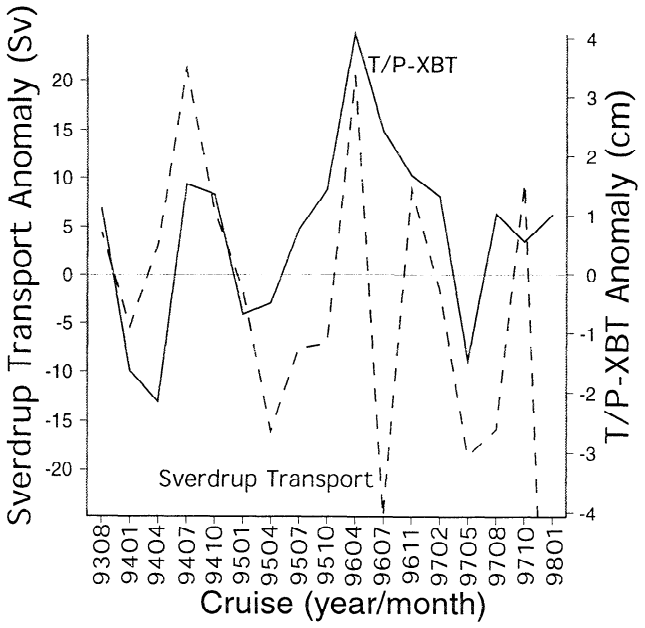

Figure 9a. Time-dependent spatial averages of difference between T/P SSH and PX50 (South Pacific) XBT dynamic height anomalies (T/P-XBT; solid line) and Sverdrup transport anomaly at 32°S (dashed line) determined from the winds in the South Pacific subtropical gyre. Positive anomalies indicate more northward transport, and negative anomalies indicate less northward transport.

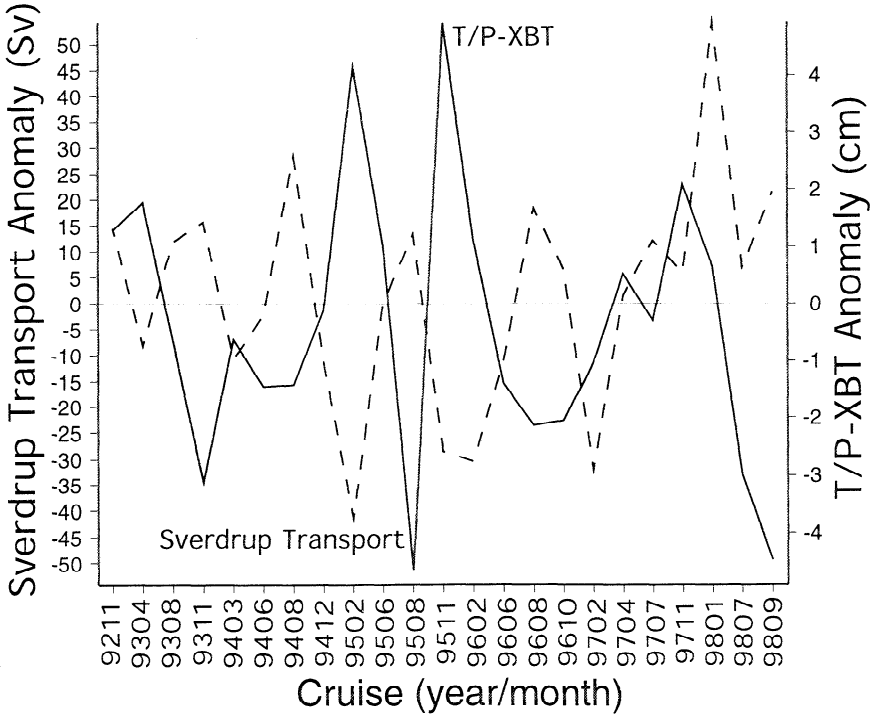

Figure 9b. Time-dependent spatial averages of difference between T/P SSH and PX37 (North Pacific) XBT dynamic height anomalies (T/P-XBT; solid line) and Sverdrup transport anomaly at 20°N (dashed line) determined from the winds in the North Pacific subtropical gyre. Positive anomalies indicate less southward transport (more northward transport) and negative anomalies indicate less northward transport.

measurement error. This indicates a dynamic origin for the observed differences. Changes in the basin mean dynamic height differences could arise from changes in mass storage or from differential density changes with depth. In sections 3.3.1 and 3.3.2 the spatially averaged SSH differences and zonal slope differences, related to meridional transport changes, are compared with Sverdrup transport anomalies at 32°S and with the spatially averaged 6°C isotherm depth anomalies to investigate dynamical causes of the differences.

3.3.1. T/P-XBT and Sverdrup transport anomalies. The Sverdrup transport anomalies at 32°S are compared to the T/P-XBT anomaly differences in Figure 9a. T/P-XBT is positive (T/P SSH has a larger positive anomaly or a smaller negative anomaly than XBT dynamic height) when the wind stress curl indicates more northward transport. Transport is always northward at this section; the mean is ~25 Sv, and the magnitude of the anomalies is always less. The sign of the T/P-XBT difference implies mass storage and/or a warming below 750 m during gyre spinup. The lack of phase lag suggests that this response is barotropic. This relation is also observed along the XBT transect PX37 near 20°N across the subtropical gyre of the North Pacific investigated by *Gilson et al.* [1998] (Figure 9b). Note that the sign is reversed in the Northern Hemisphere because a gyre spinup yields more southward (negative) transport. *Isoguchi et al.* [1997] found that the average T/P SSH (with steric component removed) across the subpolar North Pacific gyre decreases when the cyclonic gyre strengthens because of increased wind stress curl. (*Isoguchi et al.* [1997] actually removed the area-averaged steric signal, and therefore the signal examined still contains the spatial steric signal. However, the spatial and temporal pattern indicates that the remaining steric signal is not the dominant contribution.) *Stammer* [1997b] found that the SSH anomalies are relatively in phase with those of the wind stress curl over most latitudes after the steric component had been removed from the SSH, and *Ponte* [1999] found a similar relationship between bottom pressure and wind stress curl in the *Semtner and Chervin* [1992] model. While the relationship between the bottom pressure and SSH is complex, *Ponte* [1999] attributes the bottom pressure signal to mass storage. Since mass storage is a process that effects SSH, his observation provides indirect evidence that is similar to our observations. Thus the relationship between mean dynamic height and wind stress curl appears to be quite robust. An attempt to use a linear regression of the transport anomalies to correct the differences between the XBT and T/P data yielded only marginal improvement; the RMS difference between them was reduced by ~2.5 mm.

The Sverdrup transport anomalies are related to zonal slope differences between XBT dynamic height and T/P SSH as shown above and in Figure 7, with increased wind forcing creating larger meridional transport than can be observed by the XBTs alone. The spatially averaged SSH differences indicate that there is also an overall increase in height when the subtropical gyre is more strongly forced. Inspection of the boundary conditions on each gyre implies a relationship between SSH slope and its mean value across the basin that accounts for the observed pattern. The mechanism is most readily explained for the North Pacific, which has both a subtropical and a subpolar gyre. *Isoguchi et al.* [1997 - Figure 8a] illustrated that forcing for both North Pacific gyres spins up and down simultaneously. When the gyres spin up, the meridional slopes of the southern limb of the subpolar gyre and of the northern limb of the subtropical gyre must increase (Figure 10). Considering each gyre individually, the stream function Ψ must be a constant on all boundaries to enforce the condition of no flow through the boundaries. Since $\Psi = \frac{g\eta}{f}$ in this geostrophic formulation, where η is SSH, g is the gravitational constant, and f is the Coriolis parameter, η must also be a constant on the boundaries. The subpolar and subtropical gyres meet, and therefore the constant must be the same for both gyres. During the spinup of both gyres the constants for each gyre would change in an opposite sense if the slope changes were accomplished by changing the boundary constants (Figure 10c). This mechanism for changing the slope would minimally affect the mean SSH but is not possible since the gyres' constant boundary stream functions must be equal. This implies that the boundary constants cannot change in time, and slope changes must be accomplished by changes in the mean SSH as shown in Figure 10d. While the South Pacific has only a subtropical gyre, the relationship between the wind-driven gyre and the mean T/P-XBT suggests that the boundary constant between the subtropical gyre and the Antarctic Circumpolar Current (ACC) also does not vary in time, forcing slope changes to be accommodated by mean SSH changes with the phase indicating a barotropic response.

While the above explains the mechanism by which the mean SSH changes, it does not account for the dynamics that cause mass storage or divergence. This explanation is alluded to by *Ponte* [1999]. While Ekman pumping is in phase with the wind stress curl, the maximum response is lagged. *Morris et al.* [1993] found the maximum response in the western South Pacific gyre to lag the forcing by 3 months. There is a hint of a similar lag in the meridional transport across these zonal sections (Figure 7), although the time series is too sparse to quantify the lag. Pumping/suction causes an immediate convergence/divergence of mass in the gyre, but the response that equilibrates the pumping/suction has a large baroclinic, and thus delayed, component. Therefore the spatially averaged SSH increase that we observe during gyre spinup with no time lag is caused by mass storage.

3.3.2. T/P-XBT dynamic height and the 6°C isotherm depth anomalies. Figure 11 shows the cycles of the spatially averaged T/P-XBT and 6°C

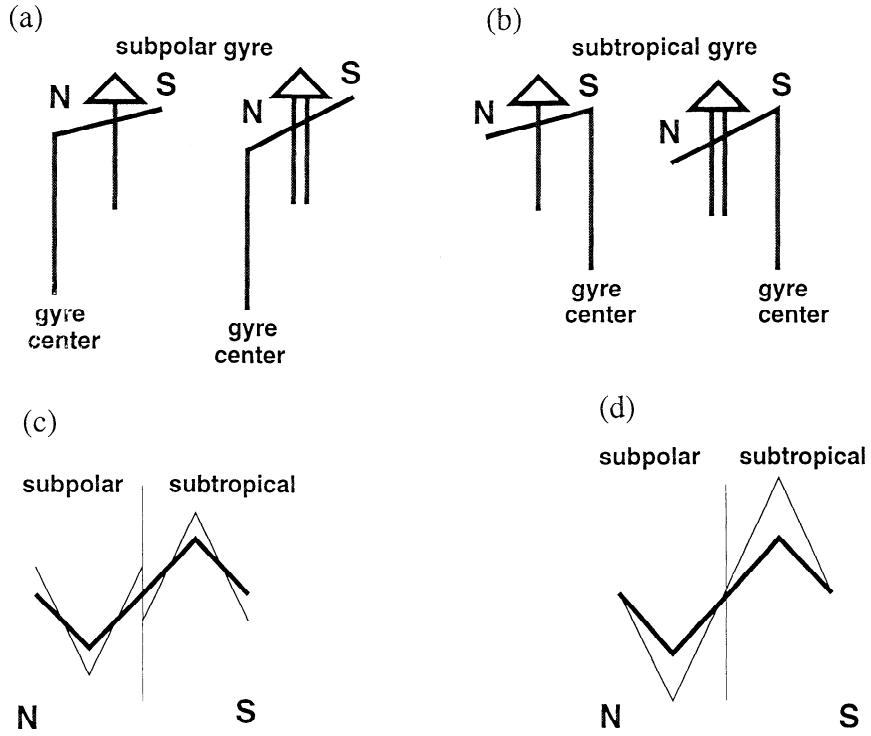

Figure 10. (a) Schematic side view of SSH of the subpolar gyre's southern limb in a mean and spun-up state. Arrows indicate flow strength. (b) Schematic side view of SSH of the subtropical gyre's northern limb in a mean and spun-up state. Arrows indicate flow strength. (c) Schematic side view of the subpolar and subtropical gyres' SSH. The thick lines indicate the mean state, and the thin lines indicate the spun-up state in which slope change is accomplished through changing boundary constants. (d) Schematic side view of the subpolar and subtropical gyres' SSH. The thick line indicates the mean state, and the thin line indicates the spun-up state in which slope change is accomplished through changing mean SSH.

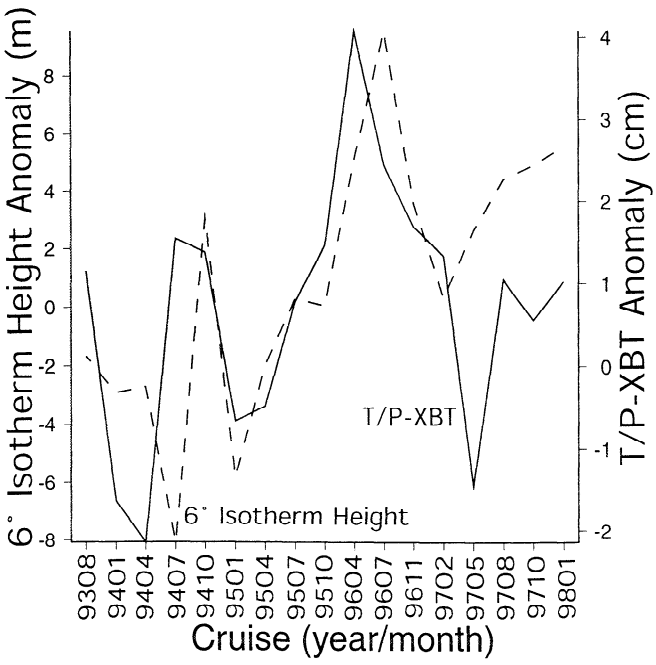

Figure 11. Time-dependent spatial averages of difference between T/P SSH and XBT dynamic height anomalies (T/P-XBT; solid line) and 6°C isotherm height anomalies (dashed line). Positive anomalies indicate a shallower 6°C isotherm.

isotherm depth anomalies. As the deepest isotherm completely captured by the XBT section, the movement of the 6°C isotherm could lend insight into the response of deeper isotherms. When T/P-XBT is negative (T/P observes a smaller positive anomaly or a larger negative anomaly than the XBTs), the 6°C isotherm is deeper than its mean depth and vice versa. That is, when the Sverdrup forcing is reduced, the 6°C isotherm is deeper than usual. If the T/P and XBT anomaly differences were due only to barotropic dynamics, we would not expect to see this pattern in isotherm movement. If the 6°C isotherm were simply responding to local increases in Ekman pumping strength, as illustrated herein with the Sverdrup forcing changes, we would expect the isotherm to deepen during gyre spinup rather than to shoal. The observed relationship also cannot be explained simply by assuming the observed warming/cooling extends deeper than 750 m. When the 6°C isotherm is deeper than average, the upper water column is warmer, thereby resulting in positive anomalies for both T/P and XBT data. If we assume the pattern extends deeper, even more of the water column would be anomalously warm, creating an even more positive T/P SSH anomaly and implying that T/P-XBT would be greater than zero. This is opposite to the observed pattern. The isotherm movement below 750 m must be

out of phase with the 6°C isotherm movement in order for the bottom part of the water column to make the negative contribution to the T/P anomaly that yields the observed pattern. The difference between XBT and T/P anomalies thus appears to have a baroclinic component with the same sign and phase.

The relationship between the XBT and T/P differences and the 6°C isotherm could be just a coincidence due to the shortness of the time series, although the robustness of the relationship suggests otherwise. Unlike the relationship between the spatially averaged differences, the zonal slope differences, and the Sverdrup transport anomalies [*Isoguchi et al.*, 1997; *Ponte*, 1999], no other observations of this negative correlation between gyre spinup and isotherm depth exist. In particular, *Morris et al.* [1996] find that the maximum 6°C isotherm depth in the western South Pacific lags the maximum pumping by ~3 months, with the winds and isotherm movement having a dominant annual cycle. At 30°S the dominant cycle is shorter than annual because this location lies between the summer and winter maximum forcing centers. A local response of the 6°C isotherm to the winds with a 2 or 3 month lag would yield an out-of-phase relationship, which is not what we observe. The possibility of baroclinic movement that is out of phase between the upper and lower portions of the water column, as suggested by the results here, remains unexplained.

4. Summary

XBT temperature sections in the South Pacific show evidence of an occasional double-gyre structure related to changes in the shallow isopycnals near the center of the gyre. XBT dynamic height and T/P SSH anomaly estimates are found to compare well with an RMS difference of 3.8 cm and a coherence of 0.7 for scales > 300 km. While the RMS difference is small, the existence of time-dependent spatially averaged differences suggests that part of the signal is due to dynamics. The relationship between T/P-XBT zonally averaged differences and the Sverdrup transport anomaly suggests that mass is stored during the gyre spinup because of a lag between the Ekman pumping and the full baroclinic response. Because of the boundary conditions, a relationship between SSH slope and mean SSH exists. The relationship between T/P-XBT zonal slope differences, i.e., the additional meridional transport observed by T/P compared with the XBTs, is also correlated with Sverdrup transport changes, as is expected if the gyre response to changing winds is deeper than that sampled by the XBTs referenced to 800 dbar. Shoaling of the 6°C isotherm during gyre spinup is observed but is unexplained and must be accompanied by deep baroclinic changes with the same period but opposite phase from the upper water column changes.

Acknowledgments. The XBT/XCTD data collection was supported by NOAA NA47GP0188 (JIMO Consortium) and NOAA NA77RJ0453 (JIMO Consortium). The analysis of TOPEX/Poseidon data was supported by NASA JPL contract 961424. NSF Ocean Sciences Division OCE 97-12209 paid for the graphics and printing. The authors would like to thank J. Andueza, D. Cutchin, B. Duffy, R. Johnson, and P. Sutton, who collected the data, and the captain and crew of the *Joana Bonita* and the *Asian Challenger*. TOPEX data were made available by L.-L. Fu at the NASA Jet Propulsion Laboratory. L. Lehman processed the XBT and T/P data. J. Gilson produced Figure 4 and provided the data for Figure 9b. M.C.M. was funded by a National Defense Science and Engineering Graduate fellowship. Thanks to two anonymous reviewers who provided insightful comments.

References

Charney, J. G., Geostrophic turbulence, *J. Atmos. Sci., 28,* 1087-1095, 1971.

Fu, L.-L., and R. A. Davidson, A note on the barotropic response of sea level to time-dependent wind forcing, *J. Geophys. Res., 100,* 24,955-24,964, 1995.

Fu, L.-L., and G. Pihos, Determining the response of sea level to atmospheric pressure forcing using TOPEX/Poseidon data, *J. Geophys. Res., 99,* 24,633-24,642, 1994.

Fu, L.-L., E. J. Christensen, C. A. Yamarone Jr., M. Lefebvre, Y. Ménard, M. Dorrer, and P. Escudier, TOPEX/Poseidon mission overview, *J. Geophys. Res., 99,* 24,369-24,382, 1994.

Gill, A. E., and P. P. Niiler, The theory of the seasonal variability in the ocean, *Deep Sea Res. Oceanogr. Abstr., 20,* 141-177, 1973.

Gilson, J., D. Roemmich, B. Cornuelle, and L.-L. Fu, Relationship of TOPEX/Poseidon altimetric height and circulation in the North Pacific, *J. Geophys. Res., 103,* 27,947-27,965, 1998.

Hanawa, K., P. Rual, R. Bailey, A. Sy, and M. Szabados, A new depth-time equation for Sippican or TSK T-7 and T-4 expendable bathythermographs (XBT), *Deep Sea Res. Part I, 42,* 1423-1451, 1995.

Hautala, S. L., D. H. Roemmich, and W. J. Schmitz Jr., Is the North Pacific in Sverdrup balance along 24°N?, *J. Geophys. Res., 99,* 16,041-16,052, 1994.

Huang, R. X., and B. Qiu, The structure of the wind-driven circulation in the subtropical South Pacific Ocean, *J. Phys. Oceanogr., 28,* 1173-1186, 1998.

Isoguchi, O., H. Kawamura, and T. Kono, A study on wind-driven circulation in the subarctic North Pacific using TOPEX/Poseidon altimeter data, *J. Geophys. Res., 102,* 12,457-12,468, 1997.

Le Traon, P. Y., J. Stum, J. Dorandeu, P. Gaspar, and P. Vincent, Global statistical analysis of TOPEX and Poseidon data, *J. Geophys. Res., 99,* 24,619-24,632, 1994.

Li, X., C. K. Shum, and B. D. Tapley, Accuracy evaluation of global ocean tide models, *Rep. CSR-96-3,* 80 pp., Cent. for Space Res., Univ. of Texas, Austin, 1996.

Minster, J.-F., C. Brossier, and P. Togel, Variation of the mean sea level from TOPEX/Poseidon data, *J. Geophys. Res., 100,* 25,153-25,162, 1995.

Mitchum, G., Comparison of TOPEX sea surface heights and tide gauge sea levels, *J. Geophys. Res., 99,* 24,541-24,554, 1994.

Morris, M., D. Roemmich, and B. Cornuelle, Observations of variability of the South Pacific subtropical gyre, *J. Phys. Oceanogr., 26,* 2359-2380, 1996.

Nerem, R. S., E. J. Shrama, C. J. Koblinsky, and B. D. Beckley, A preliminary evaluation of ocean topography from the TOPEX/Poseidon mission, *J. Geophys. Res., 99,* 24,565-24,583, 1994.

Pattullo, J. G., W. H. Munk, R. Revelle, and E. Strong, The seasonal oscillation in the sea level, *J. Mar. Res., 14,* 88-155, 1955.

Ponte, R. M., A preliminary model study of the large-scale seasonal cycle in bottom pressure over the global ocean, *J. Geophys. Res., 104,* 1289-1300, 1999.

Reid, J. L., On the total geostrophic circulation of the South Pacific Ocean: Flow patterns, tracers, and transports, *Prog. Oceanogr., 16,* 1-61, 1986.

Reid, J. L., On the total geostrophic transport of the Pacific Ocean: Flow patterns, tracers, and transports, *Prog. Oceanogr., 39,* 263-352, 1997.

Rhines, P. B., Waves and turbulence on a beta-plane, *J. Fluid Mech., 69,* 417-443, 1975.

Rhines, P. B., Geostrophic turbulence, *Annu. Rev. Fluid Mech., 11,* 401-441, 1979.

Roemmich, D., and B. Cornuelle, Digitization and calibration of the expendable bathythermograph, *Deep Sea Res., Part A, 34,* 299-307, 1987.

Roemmich, D., and B. Cornuelle, Observing the fluctuations of gyre-scale ocean circulation: A study of the subtropical South Pacific, *J. Phys. Oceanogr., 20,* 1919-1934, 1990.

Roemmich, D., and P. Sutton, The mean and variability of ocean circulation past northern New Zealand: Determining the representativeness of hydrographic climatologies, *J. Geophys. Res., 103,* 13,041-13,054, 1998.

Semtner, A. J., and R. M. Chervin, Ocean general circulation from a global eddy-resolving model, *J. Geophys. Res., 97,* 5493-5550, 1992.

Stammer, D., Global characteristics of ocean variability estimated from regional TOPEX/Poseidon altimeter measurements, *J. Phys. Oceanogr., 27,* 1743-1769, 1997a.

Stammer, D., Steric and wind-induced changes in TOPEX/Poseidon large-scale sea surface topography observations, *J. Geophys. Res., 102,* 20,987-21,009, 1997b.

Stammer, D., and C. Wunsch, Preliminary assessment of the accuracy and precision of TOPEX/Poseidon altimeter data with respect to the large-scale ocean circulation, *J. Geophys. Res., 99,* 24,584-24,604, 1994.

Stramma, L., R. G. Peterson, and M. Tomczak, The South Pacific Current, *J. Phys. Oceanogr., 25,* 77-91, 1995.

Sverdrup, H. U., M. W. Johnson, and R. H. Fleming, *The Oceans, Their Physics, Chemistry, and General Biology,* 1087 pp., Prentice-Hall, Englewood Cliffs, N.J., 1942.

Tapley, B. D., et al., The Joint Gravity Model 3, *J. Geophys. Res., 101,* 28,029-28,049, 1996.

Trenberth, K. E., W. G. Large, and J. G. Olson, The mean annual cycle in global ocean wind stress, *J. Phys. Oceanogr., 20,* 1742-1760, 1990.

White, N. J., R. Coleman, J. A. Church, P. J. Morgan, and S. J. Walker, A Southern Hemisphere verification for the TOPEX/Poseidon satellite altimeter mission, *J. Geophys. Res., 99,* 24,505-24,516, 1994.

Wunsch, C., and D. Stammer, The global frequency-wavenumber spectrum of oceanic variability estimated from TOPEX/Poseidon altimetric measurements, *J. Geophys. Res., 100,* 24,895-24,910, 1995.

Wunsch, C., and D. Stammer, Atmospheric loading and the oceanic "inverted barometer" effect, *Rev. Geophys., 35,* 79-107, 1997.

M. C. McCarthy, D. Roemmich, and L. D. Talley, Scripps Institution of Oceanography, University of California San Diego, La Jolla, CA 92093-0230. (ltalley@ucsd.edu)

(Received June 17, 1999; revised February 7, 2000; accepted February 21, 2000.)